Chinese Journal of
POLYMER SCIENCE

RESEARCH ARTICLE

https://doi.org/10.1007/s10118-024-3229-y
Chinese J. Polym. Sci. **2024**, *42*, 1948–1956

Synergistic Effect of Multi-Arm Architecture and Molecular Weight on Crystallization and Degradation Behavior of Star-Shaped Poly(lactic acid)

Nan Tian[a], Yi-Qing Li[a], Hong-Yi Gan[b], Zhen-Bo Ning[a], Ni Jiang[a*], and Zhi-Hua Gan[a*]

[a] *State Key Laboratory of Organic-inorganic Composites, Beijing Laboratory of Biomaterials, College of Life Science and Technology, Beijing University of Chemical Technology, Beijing 100029, China*
[b] *Institute of Material, Sinopec Beijing Research Institute of Chemical Industry, Beijing 100013, China*

Abstract Star-shaped poly(lactic acid)s (PLAs) with two to five arms were synthesized by ring opening polymerization using tin(II) 2-ethylhexanoate as catalyst and polyols as initiators. The effects of molecular weight together with multi-arm architecture on crystallization behavior, spherulite morphology and alkaline degradation behavior of star-shaped PLAs have been investigated. The results indicate that the multi-arm architecture interfered with spherulite growth, but promoted nucleation and alkaline degradation of star-shaped PLAs. Interestingly, with the increase of molecular weight (M_n), the crystallization rate first increased and then decreased, while the alkaline degradation rate was the opposite. The characteristic crystallization and alkaline degradation behavior of star-shaped PLAs were discussed based on the competition between segmental mobility and central core confinement.

Keywords Star-shaped poly(lactic acid); Crystallization; Spherulite morphology; Alkaline degradation

Citation: Tian, N.; Li, Y. Q.; Gan, H. Y.; Ning, Z. B.; Jiang, N.; Gan, Z. H. Synergistic effect of multi-arm architecture and molecular weight on crystallization and degradation behavior of star-shaped poly(lactic acid). *Chinese J. Polym. Sci.* **2024**, *42*, 1948–1956.

INTRODUCTION

Nowadays, plastics play an irreplaceable role in modern society. However, the application of disposable plastic products generates massive amounts of solid waste, which puts a huge burden on the environment.[1,2] Solid waste caused by synthetic plastics has become a global problem. Thus, it is urgent to find alternatives to traditional plastics. Poly(lactic acid) (PLA) is a biodegradable, renewable, and compostable plant-based aliphatic polyester that is widely regarded as a potential alternative to conventional plastics.[3–5] PLA has shown great application prospects in the fields of packaging, agriculture and biomedicine.[4] But the application is restricted by some intrinsic shortcomings, such as brittleness and low thermal resistance.[6,7]

In order to solve the above problems, chemical modification of PLA is a common method. For decades, various kinds of polylactides with complex molecular structures have been synthesized and reported, such as star-shaped, comb-shaped, dendrimer-like, branched, and hyperbranched.[8,9] Among them, star-shaped PLAs have received extensive attention due to their relatively simple preparation method and unique properties. Star-shaped PLAs are generally synthesized by a "core-first" strategy through ring-opening polymerization.[9] The polyol initiators have been utilized as the polymer cores, including glycerol, pentaerythritol, dipentaerythritol and some sugar alcohols, *etc*.[10–14] Compared with linear PLAs, star-shaped PLAs have a lower melting point and melt viscosity,[15] so they can be processed at a lower temperature.

Many researchers have reported the physical and chemical properties, crystallization and degradation behavior of star-shaped PLAs. Tsuji *et al*.[11] studied the effect of multi-arm on the physical properties and crystallization behavior with linear and 3-arm poly(L-lactide) (PLLA). The results show that for PLLA with the same molecular weight (M_n), the glass translation temperature (T_g) and cold crystallization temperature (T_{cc}) of 3-arm PLLA are higher than those of linear PLLA. This is because the branched structure reduces the chain motion of the PLLA and is excluded from the crystalline region. However, in other work, Tsuji *et al*.[13] concluded that T_g is not affected by branches, but depends on M_n. Kim *et al*.,[16] Zhao *et al*.[17] and Bikiaris *et al*.[18] found that the T_g of 4-arm and 16-21-arm PLLA was lower than that of linear PLLA. Kim *et al*. believe that star-shaped PLLA has higher chain mobility due to its larger free volume. While about the thermal and crystallization behavior, all the above works give the similar conclusion, that is, branches decreased the melting temperature (T_m) and disturbed the crystallization of PLLA. Furthermore, Tsuji *et al*.[13] approved that T_m is determined by M_n(arm) but not by M_n and that branches had no significant effect on T_m.

There are several reports regarding the degradation of star-

* Corresponding authors, E-mail: jiangni@mail.buct.edu.cn (N.J.)
E-mail: zhgan@mail.buct.edu.cn (Z.H.G.)

Received July 16, 2024; Accepted September 2, 2024; Published online November 7, 2024

shaped PLAs.[19–21] Numata *et al.*[21] studied the degradation behavior of PLA films with proteinase K and 1.0 mol/L NaOH solution. The results showed that the degradation rate was accelerated with the increase of branch number, and the enzymatic degradation of branched PLA was affected by stereochemistry. In general, the branched structure and molecular weight affect the thermal, crystallization and degradation properties of star-shaped PLAs.[9,22,23] Among them, the branched structure is relatively complex, including the chain directional change which is unvaried, and the initiator moiety as an impurity in the middle of the molecule.

In this work, we focus on the overlapping effect of molecular weight and multi-arm architecture on the crystallization behavior, spherulite morphology and alkaline degradation of PLA, because the influence of multi-arm architecture strongly depends on the molecular weight range. A series of linear and star-shaped PLAs with varying molecular weights were synthesized by ring-opening polymerization using tin(II) 2-ethylhexanoate ($Sn(Oct)_2$) as catalyst, with ethylene glycol, glycerol, erythritol and xylitol as initiators, respectively. The crystallization behavior, spherulite morphology and degradation behavior of linear and star-shaped PLAs have been investigated by differential scanning calorimetry (DSC), polarized optical microscopy (POM) and gravimetric analysis in detail.

EXPERIMENTAL

Materials

The lactide (LA) monomer purchased from PURAC (Netherlands) was recrystallized three times from ethyl acetate and vacuum dried at least 48 h before use. Toluene was dried by azeotropic distillation with sodium. $Sn(Oct)_2$ was dissolved in dehydrated toluene prior to use. Ethylene glycol was distilled over CaH_2 and stored in sealed flasks under an argon atmosphere before use. Erythritol and xylitol were dried in vacuum at 60 °C for 2 h prior to use. Glycerol, HPLC grade tetrahydrofuran (THF), lab grade methylene chloride, and lab grade methanol were used without further purification.

Synthesis of Star-shaped PLAs

The star-shaped PLAs were synthesized *via* ring-opening polymerization of LA.[24] Briefly, the monomer, initiator, toluene and $Sn(Oct)_2$ were placed into a reactor under argon atmosphere. The polymerization was carried out at 110 °C under sealed condition for 48 h. The product was purified three times by chloroform dissolution and precipitation of excess methanol. The precipitate was dried in vacuum at 40 °C.

In order to synthesize PLAs with different arms and molecular weights. Ethylene glycol, glycerol, erythritol and xylitol were used as initiators to produce linear (2a-), three-arm (3a-), four-arm (4a-) and five-arm (5a-) PLAs, respectively. The molecular weight of star-shaped PLAs was controlled by the ratio of monomer to initiator. And, the theoretical number-average molecular weight $M_{n(theor.)}/10^3$ g·mol^{-1} of PLAs were indicated by the numbers following the sample codes 2a, 3a, 4a and 5a. As an example, the linear 2-arm PLA with the theoretical molecular weight of 15×10^3 g·mol^{-1} was denoted as 2a-15.

Alkaline Degradation

To prepare amorphous samples, the samples were sandwiched between two Teflon sheets and using another 0.1 mm thick Teflon film as a spacer and pressed at 190 °C for 3 min, and then quenched immediately into liquid nitrogen for 5 min to keep the amorphous state. The specimen for degradation with dimensions of 10 mm × 10 mm × 0.1 mm was cut from melt-quenched amorphous film. The alkaline degradation was carried out in a vial filled with 5 mL of sodium hydroxide solution (0.5 mol·L^{-1}, pH=14.0). The vial was placed into a mechanical shaker with a speed of 100 r/min at 25 °C. After degrading for different times (6, 12, 18 and 24 h), the film was washed with distilled water several times and then freeze-dried under vacuum. All the dried films were weighted to determine the degradation rate. The values of weight loss were calculated from the average values of weight loss of three films. The mean errors were less than 6%.

Characterization

The molecular weight and distribution of the synthesized star-shaped PLAs were determined by Waters (Milford, MA) gel permeation chromatography (GPC) at 50 °C using a Shimadzu10A system and 10A refractive index detector with Shodex K-806 M and K-802 columns. Tetrahydrofuran (THF) was used as eluent at a flow rate of 1.0 mL/min. The system was calibrated by using polystyrene standards.

Differential scanning calorimetry (DSC) was conducted using a TA instrument DSC Q2000 equipped with a cooling accessory under a nitrogen flow of 50 mL/min. For the measurement of glass transition temperature (T_g) and melting temperature (T_m), the samples were kept at 200 °C for 3 min and then cooled to 20 °C at a speed of 45 °C/min, and reheated to 200 °C at a heating rate of 10 °C/min. The T_g was taken as the midpoint of the change in heat capacity. For isothermal crystallization tests, the specimens were rapidly cooled from 200 °C to a desired isothermal crystallization temperature (T_c) of 90–140 °C at a cooling speed of 45 °C/min. After the crystallization completed, the specimens were reheated to 200 °C at a heating speed of 10 °C/min.

The spherulitic morphology and spherulite growth rate were estimated using Nikon (Tokyo, Japan) polarized optical microscope (POM) equipped with a heating-cooling stage and a temperature controller (LK-600PM, Linkam Scientific Instruments, Surrey, UK). The films were heated to 200 °C and kept for 3 min to remove the thermal history, and then cooled to T_c at a speed of 45 °C/min for isothermal crystallization.

RESULTS AND DISCUSSION

Synthesis and Characterization

To investigate the effect of molecular weight and multi-arm architecture on the crystallization behavior, spherulite morphology and degradation behavior of polymers, a series of star-shaped PLAs with different molecular weights were synthesized. The molecular weight of star-shaped PLA was controlled by regulating the molar ratio of monomer to sugar alcohol in feed. The multi-arm architecture was confirmed by ^{1}H-NMR as our previous work[24]. The number-average molecular weights (M_n) and polydispersity (M_w/M_n) of star-shaped PLAs used in this study are summarized in Table 1. From the GPC results, unimodal distribution was found for all the synthetic samples and the polydispersity was between 1.17 and 1.35. In addition, it was found

https://doi.org/10.1007/s10118-024-3229-y

Table 1 Molecular characteristics and thermal properties of 2a-, 3a-, 4a- and 5a- PLAs.

Sample	$M_n^{theor.}$(g·mol^{-1})	M_n^{GPC} (g·mol^{-1})	PDI^{GPC}	T_g^{DSC} (°C)	T_m^{DSC} (°C)
2a-15	15.0×10^3	16.6×10^3	1.33	53.9	162.2
2a-30	30.0×10^3	32.2×10^3	1.19	56.6	166.8
2a-45	45.0×10^3	44.3×10^3	1.28	57.1	170.8
2a-60	60.0×10^3	73.8×10^3	1.24	58.6	173.9
3a-15	15.0×10^3	12.1×10^3	1.23	49.8	146.7
3a-30	30.0×10^3	33.3×10^3	1.35	55.5	164.9
3a-45	45.0×10^3	41.2×10^3	1.32	55.7	168.4
3a-60	60.0×10^3	73.5×10^3	1.19	59.2	171.2
4a-15	15.0×10^3	15.4×10^3	1.17	51.9	148.0
4a-30	30.0×10^3	32.1×10^3	1.25	54.9	161.1
4a-45	45.0×10^3	45.7×10^3	1.29	55.7	165.1
4a-60	60.0×10^3	69.8×10^3	1.22	58.2	167.1
5a-15	15.0×10^3	14.7×10^3	1.19	51.1	147.2
5a-30	30.0×10^3	31.9×10^3	1.21	52.0	155.1
5a-45	45.0×10^3	48.7×10^3	1.19	57.3	161.6
5a-60	60.0×10^3	71.9×10^3	1.23	58.4	167.7

that the molecular weight of PLAs increased with the increase of the theoretic molecular weight.

Thermal Properties of Star-shaped PLAs

Fig. 1 shows the typical DSC heating curves of PLAs after cooling. As listed in Table 1, the T_m and T_g of star-shaped PLAs are in the temperature range of 145–175 °C and 48–60 °C, respectively, and both increase with the increase of molecular weight.

To compare the effect of multi-arm architecture on T_m and T_g of PLAs, T_m and T_g as functions of M_n and M_n per arm (M_n (arm)) are plotted in Fig. 2. It can be found that in the case of similar M_n, the T_m value gradually decreases with the increase of arm number, while in the case of similar M_n (arm), the T_m value of PLA with different arms is similar. This result indicates that the crystalline thickness of star-shaped PLAs is determined by M_n (arm) but not M_n, as reported by Tsuji *et al.*[13], and the multi-arm architecture does not affect the crystalline thickness of PLAs.

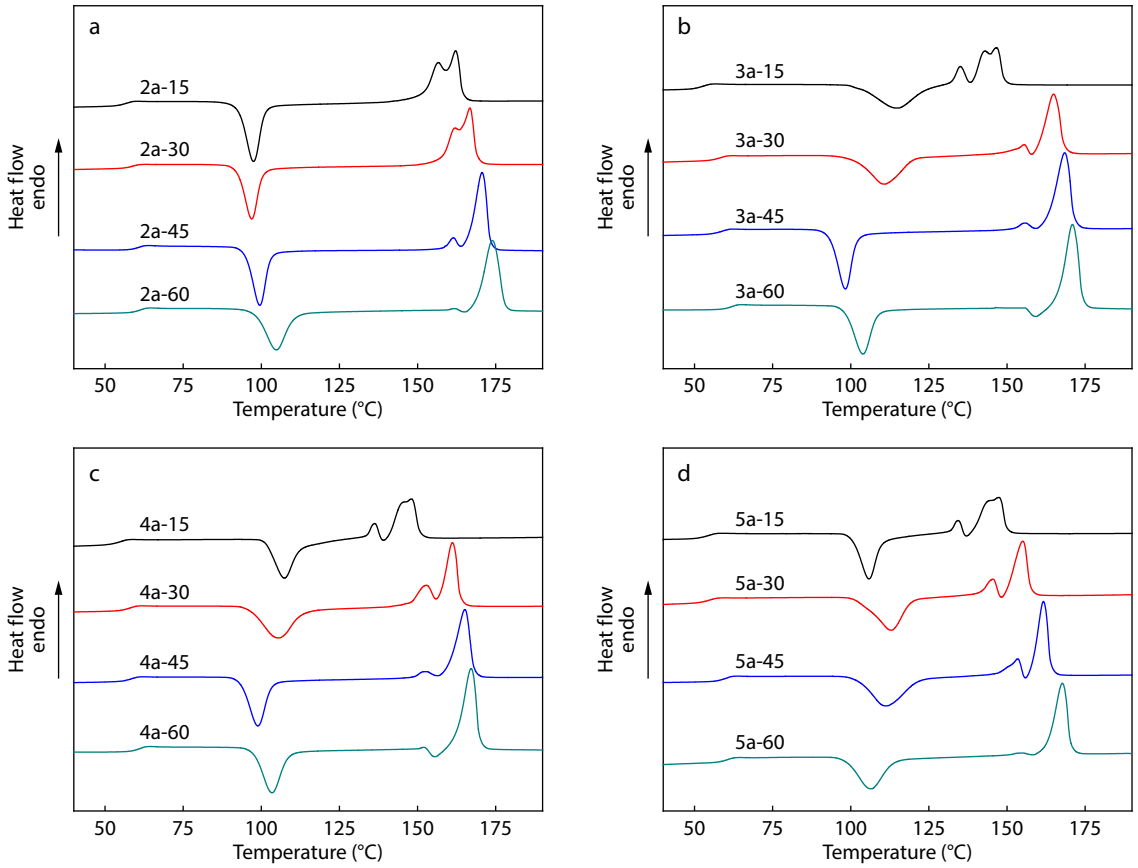

Fig. 1 DSC heating thermograms of PLAs with a heating rate of 10 °C/min after cooling.

https://doi.org/10.1007/s10118-024-3229-y

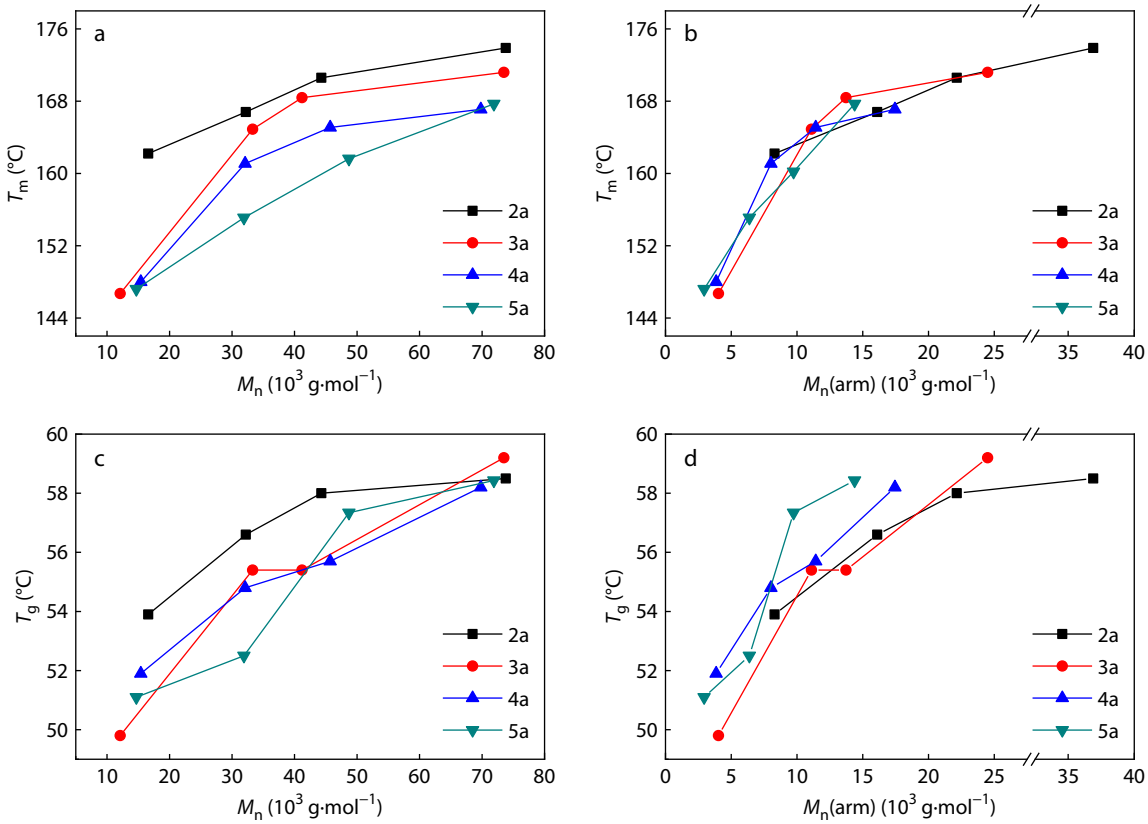

Fig. 2 The T_m and T_g of star-shaped PLAs as functions of M_n (a, c) and M_n (arm) (b, d).

As to the T_g values, the influence factors are a little complex. The T_g of linear 2a-PLAs were higher than those of star-shaped PLAs when compared at similar M_n but lower when compared at similar M_n (arm) (see Figs. 2c and 2d). By changing the chain architecture from linear to multi-arm, the central core and the chain ends are the two main factors that affect T_g.[18] For star-shaped PLAs with the same molecular weight but different arm numbers, more number of arms result in decreased arm length and more chain ends. In this case, on one hand, the limitation of central core on the segmental mobility of each arm would increase. On the other hand, the segmental mobility of molecular chains would increase because the mobility of chain ends is higher than the middle part of the chain.[25,26] With the increase of M_n, the effects of both central core and chain ends on the segmental mobility would be weaken, this is why the T_g differences decreased with the increase of the molecular weight. For PLAs with the same arm length, the effect of the chain ends on the segmental mobility is similar, but the limitation from the central core would increase with more arms. Therefore, the T_g of PLAs would become higher with the increase of the arm number at the same arm length.

Isothermal Crystallization Behavior

The crystallization behavior is extremely important for processing and industrial application of polymers.[27,28] Thus, the isothermal crystallization of star-shaped PLAs was studied in detail. Crystallization half-time ($t_{1/2}$) is the time required to reach a relative crystallization degree of 50%. The shorter $t_{1/2}$ means the faster the crystallization rate. The dependence of $t_{1/2}$ value on supercooling degree ($\Delta T = T_m - T_c$) of PLAs are shown in Fig. 3. It can be seen clearly that all the curves are unimodal, and the ΔT corresponding to the fastest crystallization rate is in the temperature range of 40–50 °C for relatively low molecular weight PLAs and 60–70 °C for relatively high molecular weight PLAs.

To investigate the effect of multi-arm architecture on the crystallization rate of PLA, the curves of $t_{1/2}$ versus M_n or M_n(arm) after isothermal crystallization at ΔT=40 °C were shown in Fig. 4. It was found that for star-shaped PLAs with similar molecular weights, the $t_{1/2}$ value increases with the number of arms, whether as a function of M_n or M_n(arm) except for 5a-60. On one hand, the more chain ends result in higher chain mobility which can increase the crystallization rate. Besides, the nucleation effect of central core increased with the number of arms which can be seen clearly from the following Fig. 5. On the other hand, the more chain directional change and more complex initiator structure as an impurity can decelerate the spherulite growth rate.[9,11,29,30] The results suggested that the confinement on the crystallization from the central core plays a significant role in affecting the crystallization rate. For 5a-60, the nucleation effect is much stronger as shown in Fig. 5, which is why its $t_{1/2}$ is much lower. Similarly, for star-shaped PLAs with similar arm length, the crystallization rate also decreased with the increase of arm number due to the limitation of the central core.

In addition, it can be found from Fig. 4(a) that the $t_{1/2}$ value of PLAs crystallized at the same ΔT decreases first and then increases with the increase of M_n. This is different from the law that the crystallization rate of single-arm polymers decreases

https://doi.org/10.1007/s10118-024-3229-y

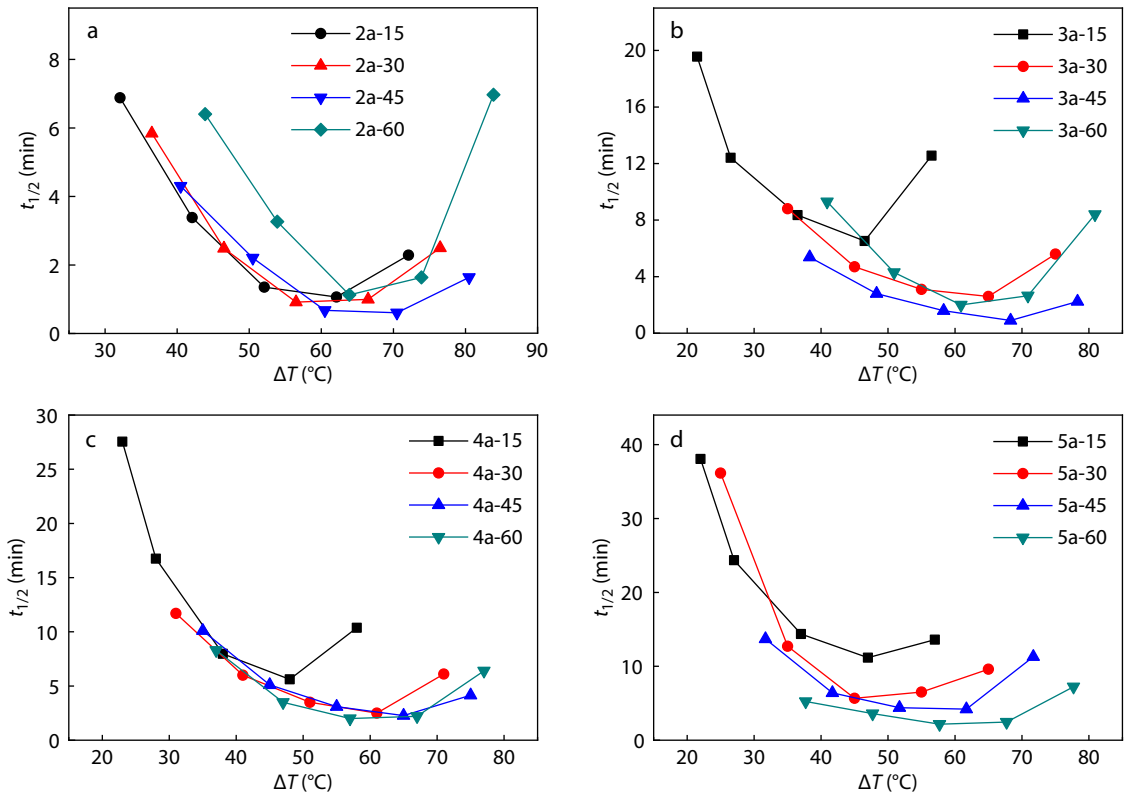

Fig. 3 The $t_{1/2}$ of PLAs at different supercooling degrees ΔT.

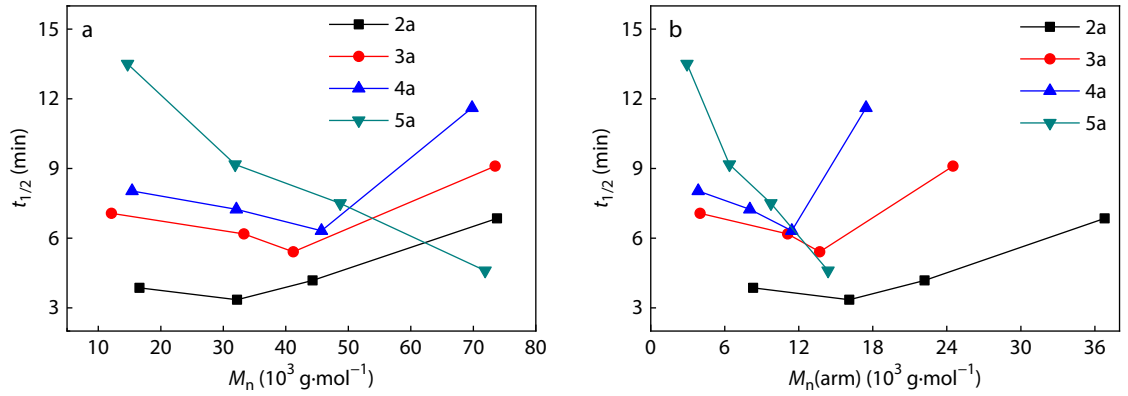

Fig. 4 Crystallization half-time as a function of (a) M_n or (b) M_n(arm) for star-shaped PLA samples after isothermal crystallization at the same ΔT (40 °C).

with the increase of molecular weight.[31,32] Here, both the central core and the molecular weight affect the crystallization rate of PLAs. By increasing M_n, the viscosity of polymers would increase. Therefore, the segmental mobility would decrease, which would result in the decrease of crystallization rate. But at the same time, the confinement from the central core on the movement of polymer chains would decrease. The results indicated that for star-shaped PLAs with M_n below a certain value, the decreased confinement from the central core with the increase of M_n is dominant. While for PLAs with M_n above a certain value, the decreased segmental mobility from the high viscosity with the increase of M_n is dominant. Besides, it could be found that the M_n corresponding to the lowest $t_{1/2}$ value increases with the number of arms (about 30×10^3, 45×10^3, 45×10^3 and $\geq60\times10^3$ g·mol^{-1} for 2a-, 3a-, 4a-, and 5a-PLAs, respectively), which may be related to the fact that PLA with more arms is more constrained by the central core.

For star-shaped PLAs with the same number of arms, the variation rule of $t_{1/2}$ with M_n(arm) is similar to that with M_n, as shown in Fig. 4(b). However, the M_n(arm) corresponding to the lowest $t_{1/2}$ value decreases with the increase of arm number (about 15×10^3, 15×10^3, and 11.25×10^3 g·mol^{-1} for 2a-, 3a-, and 4a-PLAs, respectively) except for 5a-PLAs. This should be assigned to the higher viscosity of PLAs with the much higher molecular weight.

Spherulitic Morphology and Radial Growth Rate

Fig. 5 shows the spherulite morphologies of all the star-shaped

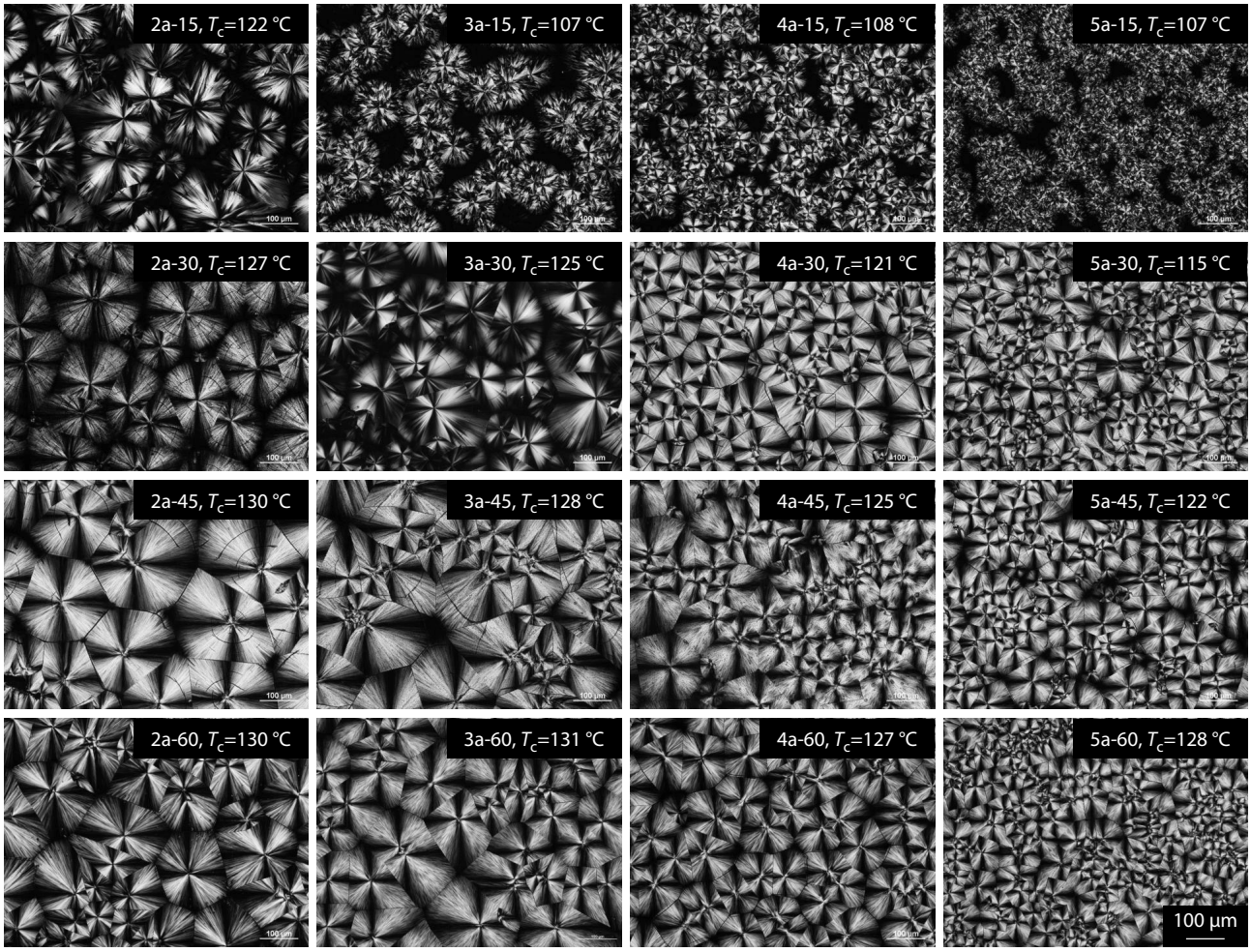

Fig. 5 POM micrographs of star-shaped PLAs spherulites after melt-crystallized at different T_c (ΔT=40 °C).

PLAs isothermally crystallized at ΔT=40 °C. It was found that the spherulites of star-shaped PLAs with similar molecular weights become smaller and more irregular as the number of arms increase. Due to the same ΔT, the difference in spherulite size and spherulite density should be assigned to the multi-arm structure. Thus, it could be concluded that the central cores can act as heterogeneous nucleation sites, the more arms, the higher nucleation ability.

Fig. 6 shows the relationship between the radial spherulite growth rate (G) of the star-shaped PLAs at ΔT=40 °C and M_n or M_n(arm). It was found that for PLAs with similar molecular weights, whether it as a function of M_n or M_n(arm), the G value decreases as the number of arms increase, indicating that the multi-arm structure disturbs the spherulite growth of PLAs. It can be seen from Fig. 6(a) that with the increase of M_n, the G value of star-shaped PLAs first increases and then decreases, and the M_n corresponding to the maximum G value is around 45×10^3 g·mol^{-1}. As shown in Fig. 6(b), the G values also increase first and then decrease with the increase of M_n(arm). However, the M_n(arm) corresponding to the maximum G value decreased with the increase of arm number (about 22.5×10^3, 15×10^3, 11.25×10^3 and 8.75×10^3 g·mol^{-1} for 2a-, 3a-, 4a- and 5a-PLAs, respectively). The results are in consistent with those obtained in Fig. 4. The deviation between the two results reflects the difference of crystallization rate and spherulite growth rate. The former is not only determined by the latter, but also by the nucleation rate.

Alkaline Degradation

It has been reported that the degradation rate of crystalline polymer is strongly affected by crystallinity and crystal structure.[33–36] Therefore, to avoid the influence of crystallization on the degradation behavior of PLAs, amorphous films prepared by melt-quenching were used for alkaline degradation. The results of PLAs with a molecular weight of 15×10^3 g·mol^{-1} are not compared because they are too brittle to form films. For all star-shaped PLAs, it was found that the molecular weight and polydispersity did not change significantly during the alkaline degradation process (for simplicity, only the results of PLAs with similar M_n of 30×10^3 g·mol^{-1} are selectively listed in Table 2). The results indicated that alkaline degradation does not occur in the central core of the PLAs, but may preferentially occur at the chain ends. The similar conclusion was also reported by Numata *et al.*[21]

To clarify the effect of molecular weight on the alkaline degradation of PLAs, Fig. 7 shows the weight loss of different films over time. It could be found that the degradation rate of all star-shaped PLAs with the same arm number decreased first and then increased with the increase of M_n, and the turn-

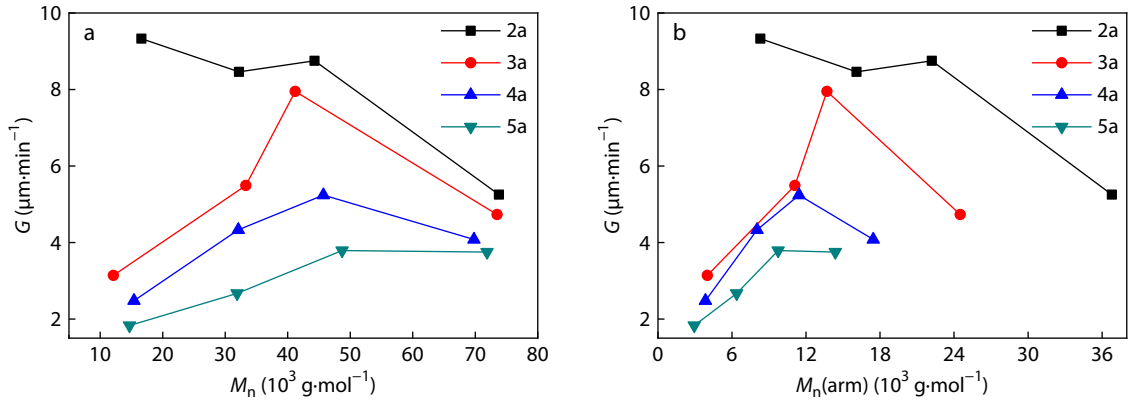

Fig. 6 The relationship between the spherulite radial growth rate and M_n (a) or M_n(arm) (b) of star-shaped PLAs during melt crystallization at ΔT=40 °C.

Table 2 Molecular weight (polydispersity) of star-shaped PLAs before and after alkaline degradation for different time.

Sample	Alkaline degradation time				
	0 h	6 h	12 h	18 h	24 h
2a-30	32.3×10^3 (1.19)	33.2×10^3 (1.18)	31.5×10^3 (1.19)	32.5×10^3 (1.17)	31.6×10^3 (1.18)
3a-30	33.3×10^3 (1.35)	31.3×10^3 (1.33)	33.5×10^3 (1.33)	34.9×10^3 (1.33)	33.4×10^3 (1.30)
4a-30	32.1×10^3 (1.25)	31.2×10^3 (1.26)	33.5×10^3 (1.24)	34.7×10^3 (1.17)	33.5×10^3 (1.16)
5a-30	31.9×10^3 (1.21)	29.6×10^3 (1.20)	32.2×10^3 (1.19)	33.3×10^3 (1.18)	31.8×10^3 (1.18)

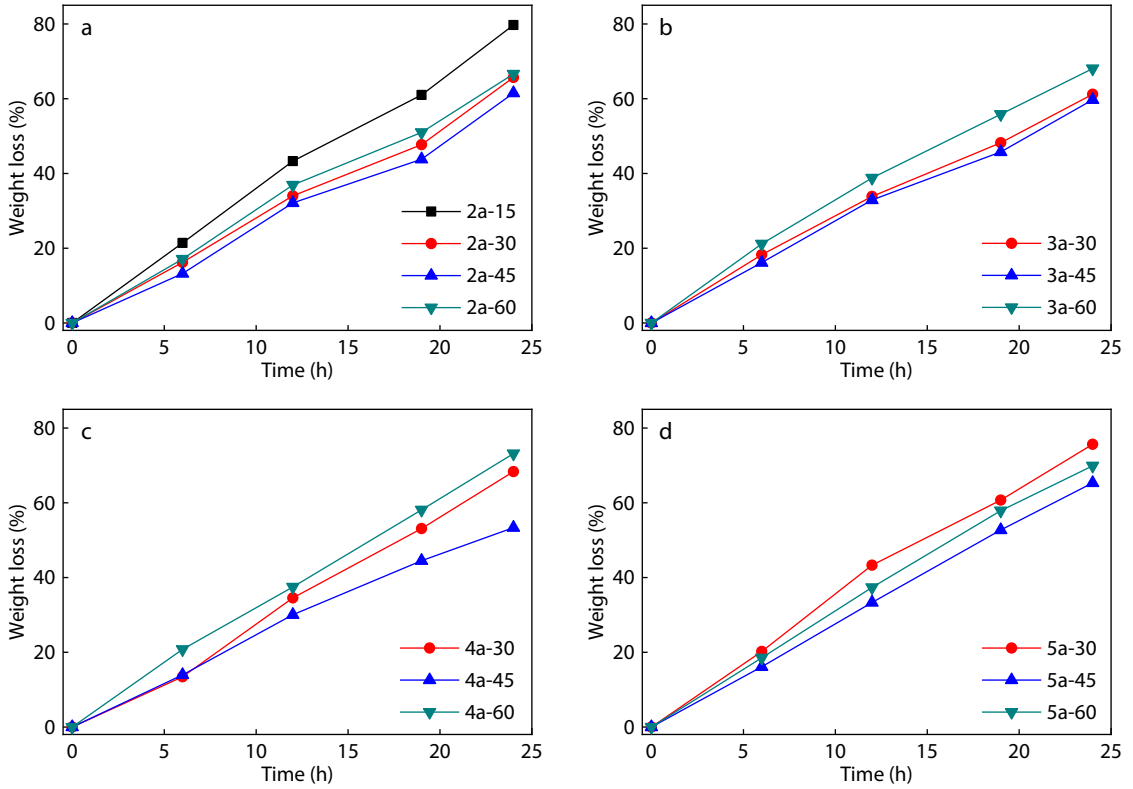

Fig. 7 Weight loss of star-shaped PLAs during alkaline degradation.

ing M_n is in the vicinity of 45×10^3 g·mol^{-1}. As mentioned above, the restricted segmental mobility at higher M_n would result in a slower degradation rate. Meanwhile, the restriction of segmental motion contributed by the polymer core would decrease, with increasing M_n, which actually accelerate the alkaline degradation. These results indicated that for star-shaped PLAs with M_n below a certain value, the reduction segmental mobility related to M_n is the key determining factor of the degradation rate. While for PLAs with the M_n above a certain value, the decreased movement confinement from the central core with the increase of M_n is dominate.

Further, the weight loss over time for the star-shaped PLAs

https://doi.org/10.1007/s10118-024-3229-y

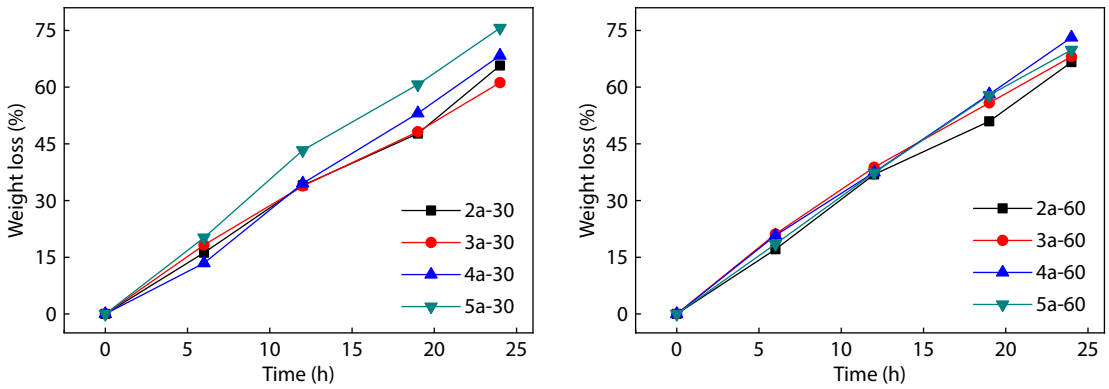

Fig. 8 Weight loss of star-shaped PLAs with similar molecular weights but different number of arms during alkaline degradation.

with similar M_n but different arm numbers is shown in Fig. 8. It can be found that for star-shaped PLAs with relatively low-molecular-weight (30×10^3 g·mol^{-1}), the alkaline degradation rate increased with the increase of arm number. Conversely, for PLAs with relatively high-molecular-weight (60×10^3 g·mol^{-1}), the degradation rate was similar. For star-shaped PLAs with similar molecular weight but different arm numbers, more branched chains mean shorter arm length and the more chain ends. Considering that the alkaline degradation preferentially takes place at the chain ends, as we pointed out in the previous, the more chain ends in star-shaped PLAs would make the degradation rate accelerate. However, the degradation rate could simultaneously decelerate due to the stronger confinement from central core on account of the shorter arm lengths. By comparing these two factors, it can be seen that the acceleration effect of the chain ends plays a dominant role in degradation. With the increase of M_n, the effects of central core and chain ends on alkaline degradation is weakened, which is why the differences of degradation rate becomes less obvious for relatively high-molecular-weight PLAs.

CONCLUSIONS

In this study, a series of well-defined star-shaped PLAs with two to five arms were successfully synthesized by ring-opening polymerization with polyols as initiators. The crystallization behavior, spherulite morphology and alkaline degradation behavior of star-shaped PLAs were investigated by DSC, POM and gravimetry analysis. It was found that the T_m, which is an indicator of crystalline thickness, is determined by M_n(arm) but not M_n, suggesting that the multi-arm architecture does not affect the crystalline thickness of PLAs. The T_gs of linear 2a-PLAs were higher than those of multi-arm PLAs when compared at similar M_n but lower when compared at similar M_n(arm) due to the complex effect of central core and chain ends.

For the crystallization of star-shaped PLAs, multi-arm architecture disturbs spherulite growth, but promotes nucleation, and the effect becomes insignificant with the increase of M_n. With the increase of ΔT, the crystallization rate of star-shaped PLAs reaches a maximum value, which is attributed to the competition between the increased chain mobility and the reduced nucleation rate. With the increase of M_n, the crystallization rate reaches a maximum value, and the corresponding M_n increases with the increase of arm number. These results are associated to the decreased confinement from central core and the decreased segmental mobility by increasing M_n. For the degradation of star-shaped PLAs, the multi-arm architecture promotes the alkaline degradation, but the influence becomes insignificant with the increase of M_n. The degradation rate of star-shaped PLAs with the same arm number reaches the minimum value with the increase of M_n, corresponding to M_n in the vicinity of 45×10^3 g·mol^{-1}, which is also ascribed to the competition between the decreased confinement from central core and the decreased segmental mobility by increasing M_n.

Conflict of Interests

The authors declare no interest conflict.

ACKNOWLEDGMENTS

This work was financially supported by the National Natural Science Foundation of China (No. 51973010).

REFERENCES

1 Prismantoko, A.; Karuana, F.; Nugroho, A.; Santoso, P. A.; Putra, H. P.; Darmawan, A.; Muflikhun, M. A.; Pranoto, I.; Aziz, M.; Hariana, H. Effects of biodegradable- and non-biodegradable-rich waste separation on ash deposition behaviour during coal and refuse-derived fuel co-combustion. *Waste Management* **2024**, *177*, 158–168.
2 Kabir, E.; Kaur, R.; Lee, J.; Kim, K. H.; Kwon, E. E. Prospects of biopolymer technology as an alternative option for non-degradable plastics and sustainable management of plastic wastes. *J. Cleaner Production* **2020**, *258*, 120536.
3 Karamanlioglu, M.; Preziosi, R.; Robson, G. D. Abiotic and biotic environmental degradation of the bioplastic polymer poly(lactic acid): a review. *Polym. Degrad. Stabil.* **2017**, *137*, 122–130.
4 Kahraman, Y.; Ozdemir, B.; Kilic, V.; Goksu, Y. A.; Nofar, M. Super toughened and highly ductile PLA/TPU blend systems by *in situ* reactive interfacial compatibilization using multifunctional epoxy-based chain extender. *J. Appl. Polym. Sci.* **2021**, *138*, 50457.
5 Yu, D. Z.; Duan, Z. P.; Wang, A. M; Li, L.; Guo, H. Y.; Deng, B. Y.; Li, D. W.; Li, H. X.; Liu, Q. S. Structure and properties of chlorogenic acid-loaded polylactide fiber prepared by melt spinning. *Int. J. Biol. Macromol.* **2024**, *265*, 130810.

6 Kervran, M.; Vagner, C.; Cochez, M.; Ponçot, M.; Saeb, M. R.; Vahabi, H. Thermal degradation of polylactic acid (PLA)/polyhydroxybutyrate (PHB) blends: a systematic review. *Polym. Degrad. Stabil.* **2022**, *201*, 109995.
7 Razavi, M.; Wang, S. Q. Why is crystalline poly(lactic acid) brittle at room temperature. *Macromolecules* **2019**, *52*, 5429−5441.
8 Nouri, S.; Dubois, C.; Lafleur, P. G. Synthesis and characterization of polylactides with different branched architectures. *J. Polym. Sci., Part B: Polym. Phys.* **2015**, *53*, 522−531.
9 Michalski, A.; Brzezinski, M.; Lapienis, G.; Biela, T. Star-shaped and branched polylactides: synthesis, characterization, and properties. *Prog. Polym. Sci.* **2019**, *89*, 159−212.
10 Wang, L.; Cai C.; Dong, C. M. Synthesis, characterization and nanoparticle formation of star-shaped poly(L-lactide) with six arms. *Chinese J. Polym. Sci.* **2008**, *26*, 161−169.
11 Tsuji, H.; Miyase, T.; Tezuka, Y.; Saha, S. K. Physical properties, crystallization, and spherulite growth of linear and 3-arm poly(L-lactide)s. *Biomacromolecules* **2005**, *6*, 244−254.
12 Belabbes, K.; Pinese, C.; Leon-Valdivieso, C. Y.; Bethry, A.; Garric, X. Creation of a stable nanofibrillar scaffold composed of star-shaped PLA network using sol-gel process during electrospinning. *Molecules* **2022**, *27*, 4154.
13 Sakamoto, Y.; Tsuji, H. Crystallization behavior and physical properties of linear 2-arm and branched 4-arm poly(L-lactide)s: effects of branching. *Polymer* **2013**, *54*, 2422−2434.
14 Han, L. L.; Shan, G. R.; Bao, Y. Z.; Pan, P. J. Exclusive stereocomplex crystallization of linear and multiarm star-shaped high-molecular-weight stereo diblock poly(lactic acid)s. *J. Phys. Chem. B* **2015**, *119*, 14270−14279.
15 Li, C. Y.; Gong, W. G.; Deng, Z. P.; Yao, Z. Y.; Meng X.; Xin Z. Fully biodegradable long-chain branched polylactic acid with high crystallization performance and heat resistance. *Indust. Eng. Chem. Res.* **2022**, *61*, 10945−10954.
16 Kim, E. S.; Kim, B. C.; Kim, S. H. Structural effect of linear and star-shaped poly(L-lactic acid) on physical properties. *J. Polym. Sci., Part B: Polym. Phys.* **2004**, *42*, 939−946.
17 Zhao, Y. L.; Cai, Q.; Jiang, J.; Shuai, X. T.; Bei, J. Z.; Chen, C. F.; Xi, F. Synthesis and thermal properties of novel star-shaped poly(L-lactide)s with starburst PAMAM-OH dendrimer macroinitiator. *Polymer* **2002**, *43*, 5819−5825.
18 Bikiaris, N. D.; Klonos, P.A.; Ioannidis, R. O.; Saranti, P.; Barmpalexis, P.; Kyritsis, A. Molecular mobility and thermal transitions study in renewable PLA-polyols star-like copolymers. *Polymer* **2024**, *292*, 126635.
19 Tsuji, H.; Hayashi T. Hydrolytic degradation and crystallization behavior of linear 2-armed and star-shaped 4-armed poly(L-lactide)s: effects of branching architecture and crystallinity. *J. Appl. Polym. Sci.* **2015**, *132*, 41983.
20 Choinska, E.; Muroya, T.; Swieszkowski, W.; Aoyagi, T. Influence of macromolecular structure of novel 2-and 4-armed polylactides on their physicochemical properties and *in vitro* degradation process. *J. Polym. Res.* **2016**, *23*, 132.
21 Numata, K.; Srivastava, R. K.; Finne-Wistrand, A.; Albertsson, A. C.; Doi, Y.; Abe, H. Branched poly(lactide) synthesized by enzymatic polymerization: effects of molecular branches and stereochernistry on enzymatic degradation and alkaline hydrolysis. *Biomacromolecules* **2007**, *8*, 3115−3125.
22 Bojda J.; Piorkowska, E.; Lapienis, G.; Michalski A. Crystallization of star-shaped and linear poly(L-lactide)s. *Eur. Polym. J.* **2018**, *105*, 126−134.
23 Xiang, S.; Jun, S.; Li, G.; Bian, X. C.; Feng, L. D.; Chen, X. S.; Liu, F. Q.; Huang S. Y. Effects of molecular weight on the crystallization and melting behaviors of poly(L-lactide). *Chinese J. Polym. Sci.* **2016**, *34*, 69−76.
24 Xie, W. Y.; Jiang, N.; Gan, Z. H. Effects of multi arm structure on crystallization and biodegradation of star-shaped poly(e-caprolactone). *Macromol. Biosci.* **2008**, *8*, 775−784.
25 Miwa, Y.; Tanase, T.; Yamamoto, K.; Sakaguchi, M.; Sakai, M.; Shimada, S. Influence of chain end and molecular weight on molecular motion of polystyrene, revealed by the ESR selective spin-label method. *Macromolecules* **2003**, *36*, 3235−3239.
26 Fukuda, J.; Adachi, K.; Tsukahara, Y.; Miwa, Y. Analysis of molecular motion around chain ends of multibranched polymers. *Chem. Lett.* **2017**, *46*, 1330−1332.
27 Nouri, S.; Lafleur, P. G.; Dubois, C. Enhanced film blowing of polylactide by incorporating branched chains and stereocomplex crystals. *Int. Polym. Proc.* **2015**, *30*, 500−510.
28 Zhao, X.; Yu, J.; Liang, X.; Huang, Z.; Li, J.; Peng, S. Crystallization behaviors regulations and mechanical performances enhancement approaches of polylactic acid (PLA) biodegradable materials modified by organic nucleating agents. *Int. J. Biol. Macromol.* **2023**, *233*, 123581.
29 Tsuji, H.; Sugiura, Y.; Sakamoto, Y.; Bouapao, L.; Itsuno, S. Crystallization behavior of linear 1-arm and 2-arm poly(L-lactide)s: effects of coinitiators. *Polymer* **2008**, *49*, 1385−1397.
30 Nouri, S.; Dubois, C.; Lafleur, P. G. Homocrystal and stereocomplex formation behavior of polylactides with different branched structures. *Polymer* **2015**, *67*, 227−239.
31 Saeidlou, S.; Huneault, M. A.; Li, H.; Park, C. B. Poly(lactic acid) crystallization. *Prog. Polym. Sci.* **2012**, *37*, 1657−1677.
32 Li, Z.; Wang, J.; Pérez-Camargo, R. A.; Müller, A. J.; Zhang, B.; Grayson, S. M.; Hu, W. Non-monotonic molecular weight dependence of crystallization rates of linear and cyclic poly(epsilon-caprolactone)s in a wide temperature range. *Polym. Int.* **2016**, *65*, 1074−1079.
33 Göpferich, A. Mechanisms of polymer degradation and erosion. *Biomaterials* **1996**, *17*, 103−114.
34 Tsuji, H.; Ikada, Y. Properties and morphology of poly(l-lactide) 4. effects of structural parameters on long-term hydrolysis of poly(l-lactide) in phosphate-buffered solution. *Polym. Degrad. Stabil.* **2000**, *67*, 179−189.
35 Li, J. X.; Niu, D. Y.; Liu, B.; Xu, P. W.; Yang, W. J.; Lemstra, P. J.; Ma, P. M. Improvement on the mechanical performance and resistance towards hydrolysis of poly(glycolic acid) *via* solid-state drawing. *Chinese J. Polym. Sci.* **2023**, *41*, 14−23.
36 Chen, Q.; Sogut, E.; Auras, R.; Kirkensgaard, J. J. K.; Uysal-Unalan, I. Hydrolysis of biobased stereocomplex polylactide: Polymorphism dependent crystals degradation and evolution of three-phase crystalline composition. *Appl. Mater. Today* **2024**, *38*, 102226.

https://doi.org/10.1007/s10118-024-3229-y